The Astrophysical Journal, 889:174 (6pp), 2020 February 1 https://doi.org/10.3847/1538-4357/ab5af8

6.7 GHz CH_3OH Absorption toward the N3 Galactic Center Point Source

Natalie O. Butterfield[1], Adam Ginsburg[2], Dominic A. Ludovici[3], Ashley Barnes[4], Riley Dunnagan[3], Cornelia C. Lang[5], and Mark R. Morris[6]
[1] Green Bank Observatory, 155 Observatory Rd, P.O. Box 2, Green Bank, WV 24944, USA; nbutterf@nrao.edu
[2] Department of Astronomy, University of Florida, P.O. Box 112055, Gainesville, FL 32611, USA
[3] Department of Physics and Optical Engineering, Rose-Hulman Institute of Technology, 5500 Wabash Ave, Terre Haute, IN 47803, USA
[4] Argelander Institute für Astronomy, University of Bonn, Auf dem Hügel 71, D-53121 Bonn, Germany
[5] Department of Physics and Astronomy, University of Iowa, 30 North Dubuque St, Iowa City, IA 52242, USA
[6] Department of Physics and Astronomy, University of California, 430 Portola Plaza, Los Angeles, CA 90095, USA
Received 2019 September 18; revised 2019 November 19; accepted 2019 November 22; published 2020 February 4

Abstract

We present evidence of 6.7 GHz methanol (CH_3OH) and 4.8 GHz formaldehyde (H_2CO) absorption toward the Galactic Center (GC) point source "N3." Both absorption features are unresolved and spatially aligned with N3. The 6.7 GHz CH_3OH contains a single-velocity component (centered at $\sim$10 km s^{-1}), while the 4.8 GHz H_2CO shows two-velocity components (centered at ~-3 and $+8$ km s^{-1}). We find that the velocities of these absorption components are similar to that of emission lines from other molecules (e.g., SiO and HC_3N) detected toward this compact source (-13 to $+25$ km s^{-1}; "N3 cloud"). The detection of these absorption features is a firm indication that some of the molecular gas in the N3 molecular cloud is on the near side of the continuum source. Analysis of the CH_3OH absorption kinematics shows a relatively large velocity dispersion (3.8 km s^{-1}) for the size scale of this feature ($<0\farcs1$, <0.01 pc at the GC), when compared with other similarly sized GC clouds in the Larson line width–size relationship. Furthermore, this line width is closer to velocity dispersion measurements for size scales of 1.3 pc, which is roughly the width of the N3 cloud (25″; 1.0 pc). We argue that this relatively broad line width, over a small cross-sectional area, is due to turbulence through the depth of the cloud, where the cloud has a presumed line-of-sight thickness of $\sim$1 pc.

Unified Astronomy Thesaurus concepts: Galactic center (565); Interstellar clouds (834); Molecular gas (1073)

1. Introduction

The 6.7 GHz CH_3OH (5_1^+–6_0^+) line is typically observed as a Class II maser. Class II masers are radiatively pumped and are therefore frequently associated with star-forming regions (e.g., Menten 1991). While detections of the 6.7 GHz CH_3OH line in *emission* are common (e.g., Menten 1991; Caswell et al. 2010; Lu et al. 2019; Rickert et al. 2019), detections in *absorption* are not. As of this paper, only a few studies have reported the 6.7 GHz CH_3OH line in absorption (e.g., Menten 1991; Impellizzeri et al. 2008; Pandian et al. 2008). Only a few of the sources in the Menten (1991) survey contained absorption features toward extended sources, all of which are located in the central region of our Galaxy, including: Sgr A-A, Sgr A-F, and the Sgr B2 complex.

The center of our Galaxy (Galactic Center; GC) is typically defined as the inner 500 pc of the Milky Way galaxy. The environment of molecular gas in the GC is more extreme than that in the Galactic disk, with higher gas temperatures ranging from 50–300 K (in comparison to 10–20 K in the disk; e.g., Mills & Morris 2013; Ginsburg et al. 2016). Molecular clouds in the GC are also observed to have broader line widths (2–30 km s^{-1} on 5–40 pc size-scales) than clouds in the Galactic disk (0.5–5 km s^{-1}; e.g., Oka et al. 2001; Heyer et al. 2009; Shetty et al. 2012). The relationship of cloud size to velocity dispersion (also known as the "Larson line width–size (σ–R) relationship") holds across a wide range of physical size scales from molecular cloud complexes to compact cloud cores (e.g., Larson 1981). Most of the recent measurements of GC cloud kinematics, across multiple size scales, use dendrogram analysis to fit the velocity dispersion and angular size of the gas components (e.g., Shetty et al. 2012; Kauffmann et al. 2017). We employ an alternative method of investigating GC gas kinematics at sub-parsec (<0.01 pc) size scales by using a 6.7 GHz CH_3OH absorption measurement toward the compact source N3.

1.1. N3 Point Source

The "N3" point source is located 14′ (33 pc) in projection from Sgr A* in a region known as the "Radio Arc" (see Figure 1, left). The N3 point source is spatially projected onto one of the Radio Arc Non-Thermal Filaments (e.g., Yusef-Zadeh & Morris 1987), but appears to be a distinct object (Figure 1, left). The nature of the N3 compact source has been a mystery for several decades (e.g., Yusef-Zadeh & Morris 1987; Ludovici et al. 2016; Staguhn et al. 2019). A recent study of this compact source determined N3 has a broken power-law spectrum, consistent with synchrotron self-absorption, and is shown to be time-variable over decade-long timescales (Ludovici et al. 2016). N3 is unresolved at 44 GHz (i.e., with a $0\farcs26 \times 0\farcs11$ beam), the highest spatial resolution in Ludovici et al. (2016), indicating a maximum size of $\sim$1000 au at a distance of 8.18 kpc (Abuter et al. 2019). Based on the arguments presented in Ludovici et al. (2016), possibilities that N3 is a young supernova, foreground active star, ultracompact H II region, or a microquasar are all ruled out.[7]

The N3 source has associated molecular emission (the "N3 molecular cloud") that appears to wrap around the compact source (Ludovici et al. 2016; Butterfield et al. 2018). The

[7] Ludovici et al. (2016) also disfavor N3 being an active galactic nucleus (AGN), but as we discuss in Section 3.2, that possibility should remain viable.

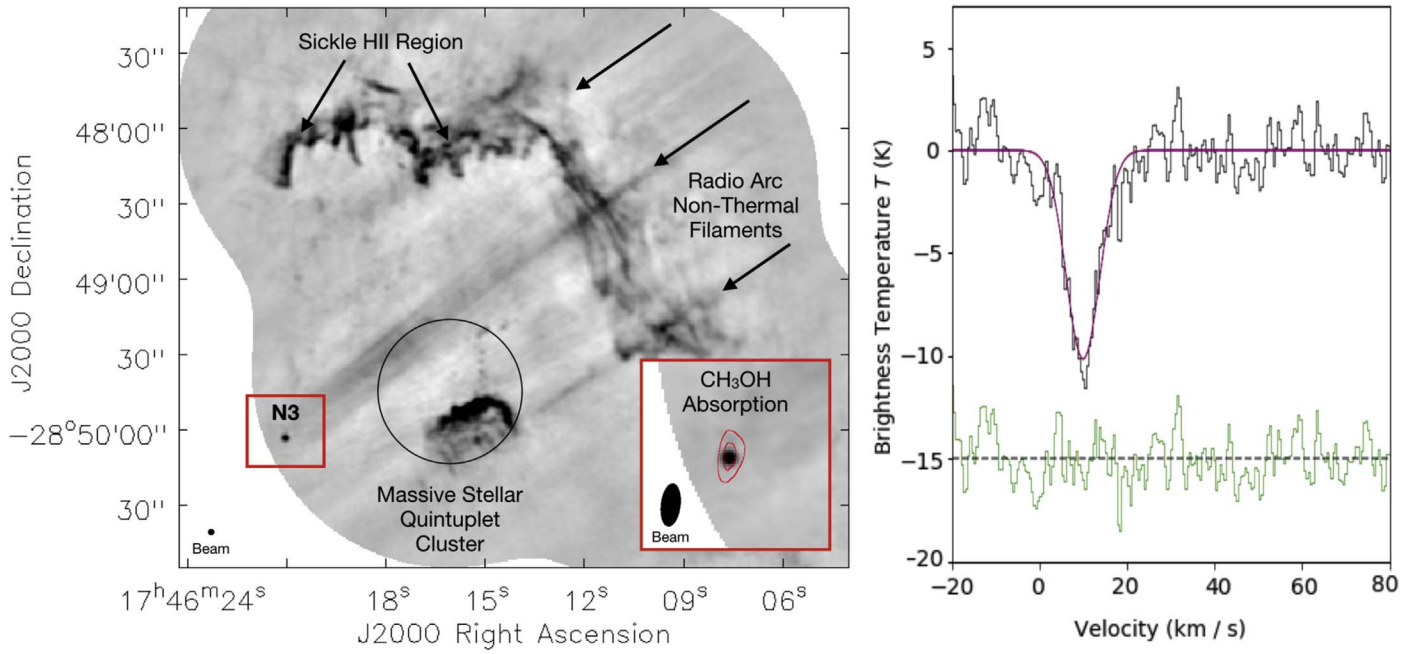

Figure 1. Left: 24.5 GHz VLA radio continuum emission showing the region around the point source N3 (Figure 2 from Butterfield et al. 2018). Several prominent radio continuum features are labeled in the figure. Among them are the Radio Arc Non-Thermal Filaments, which are discussed in Section 1.1. Inset: zoomed-in view of the 6.7 GHz CH_3OH absorption in the 9.97 km s^{-1} channel shown in red contours at −5 and −10 × 1.5 mJy beam^{-1} (rms noise; Table 1). Right: 6.7 GHz CH_3OH absorption (black spectrum) extracted using a region size comparable to the point-spread function of the data (see *inset*). The red line shows the best-fit parameters presented in Section 3.1, with the green residuals of the fit offset at −15 K.

molecular emission is extended, with a diameter of only 25″ (1.0 pc). The high gas temperatures observed in this cloud (80–100 K, Ludovici et al. 2016) suggest this cloud is located in the GC. Thermal 48 GHz CH_3OH (1_0−0_0) emission is detected in the N3 molecular cloud, along with sixteen 36 GHz CH_3OH (4_{-1}−3_0) masers and twelve 44 GHz CH_3OH (7_0−6_1) masers distributed throughout the cloud (Ludovici et al. 2016). Both of these CH_3OH maser transitions are Class I masers,[8] however, only the 36 GHz maser is spatially colocated with the radio continuum of N3.

2. Observations and Data Reduction

This paper focuses on the 6.7 GHz CH_3OH transition toward the point source N3. These observations are part of a larger "Karl G. Jansky Very Large Array," hereafter "VLA," survey of the GC (Project ID: 17A–321).[9] These observations were taken in the *C* band with the C array, resulting in a spatial resolution of ∼5″. We used the Common Astronomy Software Application (CASA)[10] pipeline, provided by NRAO, to calibrate the data. The spectral line was continuum-subtracted in the UV plane using the CASA task UVCONTSUB before any cleaning was done. The imaging parameters of the CH_3OH (5_1^+–6_0^+) data cube are presented in Table 1.

We also present the detection of 4.8 GHz H_2CO 1(1,0)–1(1,1) absorption toward N3. 4.8 GHz H_2CO absorption is known to be quite common in the GC (e.g., Whiteoak & Gardner 1979). The H_2CO data presented in this paper were taken using the VLA in the *C* band with the A array (0.″4 × 0.″8 resolution) with a sensitivity of 1.0 mJy beam^{-1} and velocity resolution of 3.88 km s^{-1} (Project ID: 18A–303). Due to the narrow velocity range, and courser spectral resolution, of the H_2CO observations, fitting the spectrum is challenging. Therefore, we will be focusing on the 6.7 GHz CH_3OH transition for the majority of the paper.

Table 1
Image and Fit Parameters

Parameter	Value
Image Parameters	
CH_3OH Rest Frequency	6.66852 GHz
Spatial Resolution	11″ × 5″ (0.4 × 0.2 pc)
Spectral Resolution	0.47 km s^{-1}
Channel Noise	1.5 mJy beam^{-1}
Fit Parameters	
Central Velocity	9.94 ± 0.17 km s^{-1}
Velocity Dispersion	3.84 ± 0.17 km s^{-1}
Depth	−10.15 ± 0.38 K

3. Results and Discussion

3.1. 6.7 GHz CH_3OH Absorption Feature

The inset in Figure 1 left shows the 6.7 GHz CH_3OH absorption in the 9.97 km s^{-1} channel. The feature is shown to be spatially aligned with the point source N3 (red contour in inset), suggesting the absorbed continuum emission is likely from N3. We extracted the CH_3OH absorption using a region size comparable to the point-spread function of the observations (11″ × 5″ aperture), with the resulting spectrum presented in the right panel of Figure 1. We fit the spectrum in Figure 1 (right panel) with a single Gaussian component, using

[8] Class I masers are *collisionally* excited and therefore trace shocks.
[9] The VLA radio telescope is operated by the National Radio Astronomy Observatory (NRAO). The National Radio Astronomy Observatory is a facility of the National Science Foundation operated under cooperative agreement by Associated Universities, Inc.
[10] http://casa.nrao.edu/

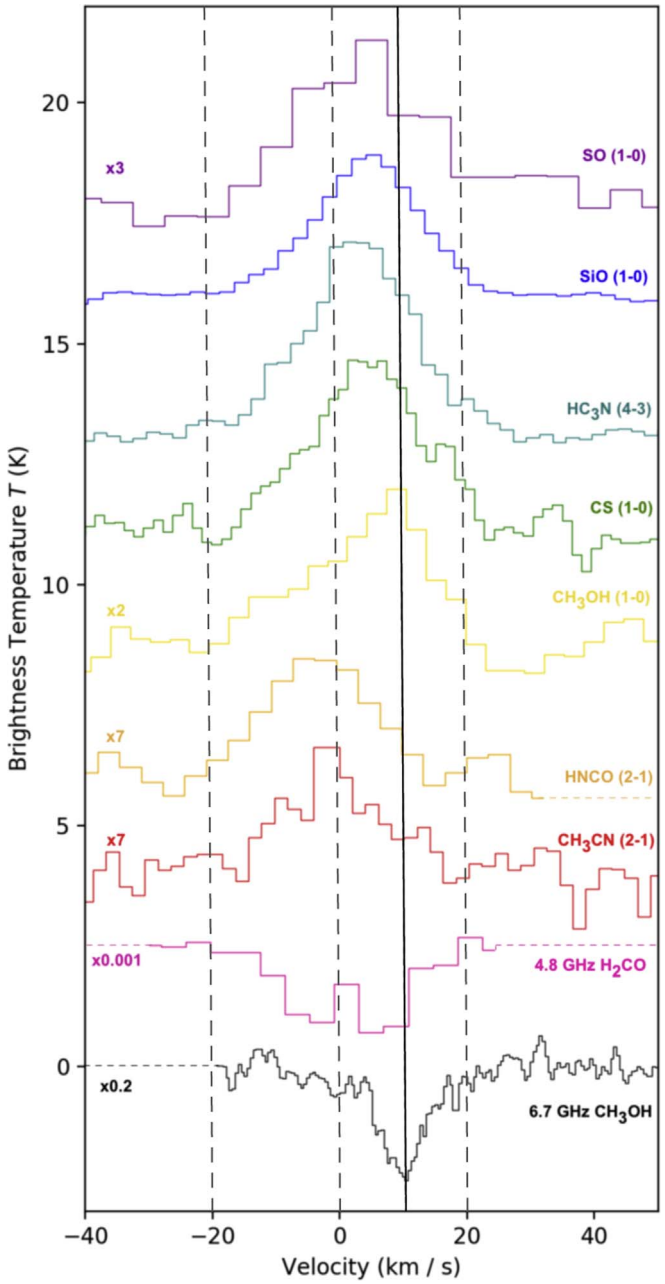

Figure 2. Comparison of the 6.7 GHz CH_3OH absorption line (black spectrum) and the 4.8 GHz H_2CO absorption (pink spectrum) to seven molecular emission lines presented in Ludovici et al. (2016; see their Table 2 and Figure 6). All spectra were integrated over the same region (3″) aperture, centered on N3: α(J2000) = $17^h46^m21\overset{s}{.}0$, δ(J2000) = −28°50′03.″9. Each spectrum is labeled with its transition on the right side. The six spectral lines that have been vertically scaled, for comparison purposes, are indicated on the left side by the multiplied value. The vertical solid black line shows the central velocity of the CH_3OH absorption line (Table 1). The three vertical gray dashed lines are reference lines at −20, 0, and +20 km s^{-1}.

the python program *pyspeckit* (Ginsburg & Mirocha 2011), and report the central velocity, velocity dispersion, and depth of the fit profile in Table 1.

The measured central velocity of the 6.7 GHz CH_3OH absorption (9.94 km s^{-1}; vertical dashed line in Figure 2) is comparable to molecular emission velocities detected in the N3 molecular cloud (−13 to +25 km s^{-1}; Ludovici et al. 2016). Figure 2 shows a comparison of the CH_3OH absorption profile (from Figure 1, right) to molecular gas emission from seven transitions in Ludovici et al. (2016) and the H_2CO absorption line presented in Section 2. The velocity range of the 6.7 GHz CH_3OH absorption feature, +5 to +15 km s^{-1}, overlaps with emission from all seven transitions (see Figure 2). However, only the CH_3OH (1_0-0_0) line (yellow spectrum) peaks at the same velocity (∼9 km s^{-1}). All other emission lines have peak emission velocities lower than the 6.7 GHz CH_3OH absorption line, with central velocities ranging from −5 to +5 km s^{-1}.

Similar to the CH_3OH absorption feature, the 4.8 GHz H_2CO absorption is also point-like and centered on N3. However, unlike the CH_3OH absorption feature, the H_2CO absorption contains two-velocity components centered roughly at −3 and +8 km s^{-1} (Figure 2). Furthermore, the large brightness temperatures in both absorption components (∼−1500 K; the brightness temperature of the H_2CO spectrum in Figure 2 was divided by 10^3 for comparison purposes), and spatial overlap with N3, suggests the absorbed continuum is likely from N3 and not the Cosmic Microwave Background.

3.2. Line-of-sight Arrangement

The detection of both CH_3OH and H_2CO absorption features indicates some of the molecular gas is located on the near side of the continuum-emitting source N3. This absorption detection opens back up a possibility ruled out in Ludovici et al. (2016). Ludovici et al. (2016) did not detect any absorption features in their spectral line study and therefore concluded the cloud is located behind N3. Furthermore, their conclusion places N3 in the GC, therefore they ruled out the possibility that N3 is a background AGN. However, the detection of absorption features in our data indicates some of the gas is located on the near side of N3 and therefore there are no physical arguments that exclude an AGN. Furthermore, the broken power-law spectrum of N3 is also consistent with SEDs of other AGNs (Ludovici et al. 2016). Thus, the possibility that N3 is a background AGN should remain viable.

3.3. CMZ Kinematics on Small Size Scales

The 6.7 GHz CH_3OH absorption feature has an unusually large velocity dispersion, 3.8 km s^{-1}, for the size scale of the continuum source N3. The *Q*-band observations in Ludovici et al. (2016) suggest an upper limit to its angular size of 0.″26, implying a maximum size scale of ∼2000 au, or ⩽0.01 pc, at a GC distance of 8.18 kpc. Figure 4 shows the line width–size relationship of clouds from multiple studies compared to the measured line width–size of the CH_3OH absorption feature (red X).

We can compare our measured velocity dispersion to the predicted velocity dispersion, for a 0.01 pc cross-section size scale, using the following equation from Kauffmann et al. (2017):

$$\sigma(v) = (5.5 \pm 1.0)\ \mathrm{km\ s^{-1}}\ (r_{\mathrm{eff}}/\mathrm{pc})^{0.66\pm0.18} \quad (1)$$

where r_{eff} is the effective radius of the region and $\sigma(v)$ is the velocity dispersion. This relationship is shown as the dashed line in Figure 3. For a 0.01 pc size scale the predicted velocity dispersion is $0.26^{+0.17}_{-0.09}$ km s^{-1}, roughly an order of magnitude *lower* than our measurements. Additionally, the measured velocity dispersion is also larger then the estimated sound speed of the gas, 0.6 km s^{-1}, using a gas temperature of ∼100 K (Ludovici et al. 2016) and Equation (1) from Kauffmann et al. (2017). This

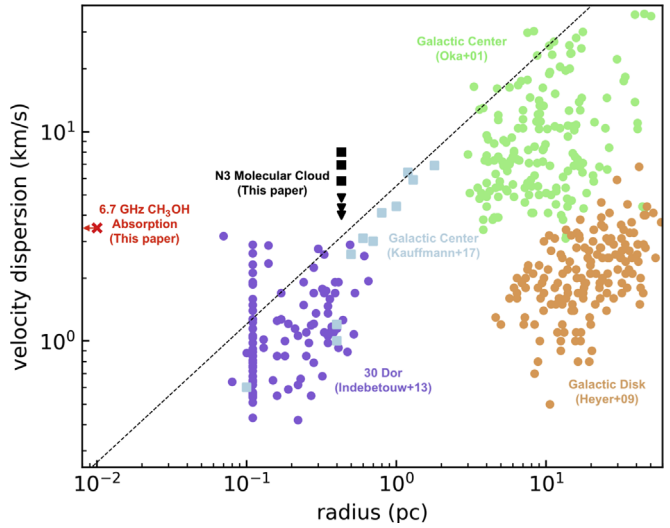

Figure 3. The Larson line width–size (σ–R) relationship of molecular clouds. The red "x" shows the absorption feature presented in Section 3.1 and discussed in Section 3.3. The black squares and triangles show the kinematics of the N3 molecular cloud for Components 1 and 2, respectively (see Table 2). The dashed line shows the expected line width–size relationship for Galactic Center clouds from Kauffmann et al. (2017; see Equation (1)). The light blue squares are from Kauffmann et al. (2017). The light green data points are from Oka et al. (2001) for gas clouds in the Galactic Center. The orange data points are from Heyer et al. (2009), showing the Galactic Disk cloud kinematics. The purple data points are from Indebetouw et al. (2013), showing measurements from 30 Doradus in the Large Magellanic Cloud.

estimated sound speed value suggests the N3 molecular cloud has a Mach number of 6, indicating the large line width is *not* produced by thermal broadening. This Mach number for the N3 cloud is comparable to other clouds in the GC that have a wide range of Mach numbers from 1.5 to 50 (e.g., Mills 2017; Kauffmann et al. 2017). The detection of a broad spectral line across such a small size scale could indicate that: (1) we are measuring turbulence along the depth of the cloud, (2) we are observing a coherently rotating cloud off-axis, or (3) N3 is a localized source that is producing the broader line width. We examine all three scenarios in the following sections.

3.3.1. Scenario 1: Turbulence along the Depth of the N3 Cloud

One possible scenario for the difference between the measured and predicted velocity dispersion values of the CH_3OH absorption feature is that we are measuring the velocity dispersion across the depth of the cloud, where the thickness of the cloud is larger than the observed cross section of the point source. If the velocity dispersion is caused by turbulence across the thickness of the cloud, then the velocity dispersion of the pencil beam through the cloud is a 1D profile. Therefore, the 3D velocity dispersion would be $\sqrt{3}$ times larger than the measured 1D velocity profile, assuming the turbulence is isotropic. In this scenario, the 3D velocity dispersion, for a 3.84 km s^{-1} 1D velocity profile, is 6.58 km s^{-1}. Using Equation (1), this velocity dispersion corresponds to a size scale of $1.3^{+1.0}_{-0.3}$ pc. The observed diameter of the N3 molecular cloud is ~10″–25″ (0.4–1.0 pc; Ludovici et al. 2016), indicating the detected velocity dispersion is roughly comparable for the size scale of the whole N3 molecular cloud. To test this idea we investigate the kinematics of the entire N3 molecular cloud.

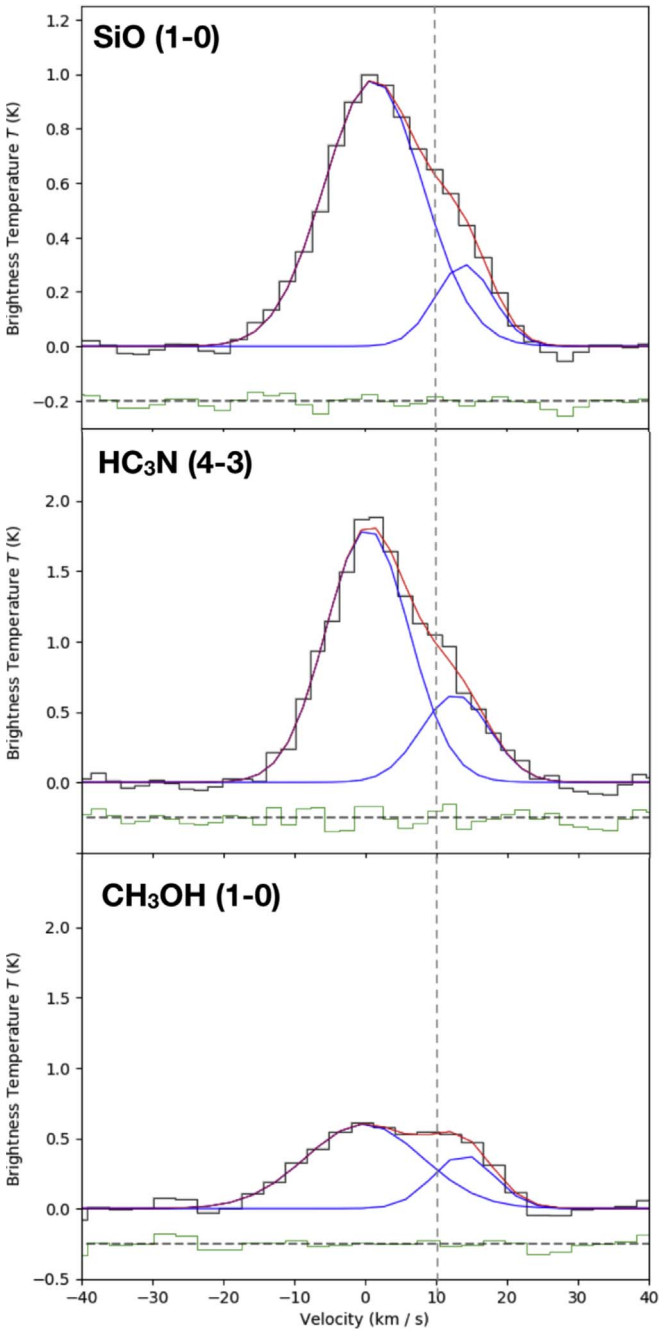

Figure 4. Black histogram shows the spectral profiles of SiO (1−0), HC_3N(4−3), and CH_3OH (1−0), from Ludovici et al. (2016), integrated over the whole cloud ($R = 11\farcs2 = 0.43$ pc; centered at α(J2000) = $17^h46^m20\fs8$, δ(J2000) = −28°50′01″). In all three panels the spectra are best fit with two-velocity components (blue Gaussians). The fitted parameters of each component for each transition are listed in Table 2. The red line shows the combined fit of the two components, with the green histogram showing the residuals of the fit. The vertical gray dashed line shows the central velocity of the 6.7 GHz CH_3OH absorption feature.

Figure 4 shows the spatially averaged SiO (1−0), HC_3N (4−3), and CH_3OH (1−0) (data from Ludovici et al. 2016, see their Figure 6) emission spectrum integrated over the whole cloud ($r_{\rm eff} = 11\farcs2 = 0.43$ pc). These spectra were also fit using the python program *pyspeckit*. The properties of the best-fit Gaussian components are listed in Table 2. All three spectra show two-velocity components in the N3 cloud; a

Table 2
Kinematics of the N3 Molecular Cloud

Parameter[a]	Component 1	Component 2
SiO (1−0)		
v_c	1.3 ± 0.7 km s^{-1}	14.1 ± 1.2 km s^{-1}
σ	7.0 ± 0.6 km s^{-1}	4.0 ± 1.0 km s^{-1}
T_B	0.98 ± 0.03 K	0.30 ± 0.08 K
HC_3N (4−3)		
v_c	0.3 ± 0.5 km s^{-1}	12.7 ± 1.2 km s^{-1}
σ	5.8 ± 0.4 km s^{-1}	4.8 ± 0.8 km s^{-1}
T_B	1.80 ± 0.06 K	0.62 ± 0.09 K
CH_3OH (1−0)		
v_c	−0.1 ± 1.2 km s^{-1}	13.9 ± 0.8 km s^{-1}
σ	8.0 ± 1.0 km s^{-1}	4.3 ± 0.8 km s^{-1}
T_B	0.60 ± 0.03 K	0.38 ± 0.09 K

Note.
[a] Where v_c is the central velocity of the component, σ is the velocity dispersion, and T_B is the peak brightness temperature.

low-velocity component around 0 km s^{-1} (Component 1), and a high-velocity component around 13 km s^{-1} (Component 2). The central velocity of Component 2 is comparable to that of the CH_3OH absorption feature, indicating the absorption could be associated with this gas component. The velocity dispersion of both components, for all three transitions, are plotted in Figure 3. In general, the N3 cloud appears to have a higher-velocity dispersion then other GC clouds on similar 0.5–1.0 pc size scales. Our measured velocity dispersion of the CH_3OH absorption feature is comparable to the velocity dispersion across the entire cloud. Therefore, the broad line width could be produced by turbulence along the depth of the cloud, where the N3 cloud has a thickness of roughly 1 pc at this location.

3.3.2. Scenario 2: Large-scale Cloud Rotation

Another scenario that could cause the large velocity dispersion detected along a pencil beam through the cloud is a large-scale cloud rotation. Observing a coherently rotating cloud off-axis could produce broad lines by blending multiple-velocity components through the rotating cloud. To investigate this idea we consider the intensity-weighted velocity distribution (moment 1) across the cloud. If the cloud were rotating we would expect to see a velocity gradient across the cloud as a signature of rotation.

Figure 5 shows the intensity-weighted velocity distribution (moment 1) across the cloud in the SiO (1−0) transition from Ludovici et al. (2016). Most of the lower-velocity emission (below 0 km s^{-1}) is located toward the edge of the cloud, with the higher-velocity emission (above 0 km s^{-1}) located toward the center of the cloud. There does not appear to be a large-scale velocity gradient across the entire cloud but rather a gradient from the "outside" inward. The absence of a large-scale velocity gradient across the cloud suggests that the large velocity dispersion is *not* due to cloud rotation.

3.3.3. Scenario 3: N3 Embedded in the Molecular Cloud

Lastly, a broad absorption feature could be produced if N3 is *embedded* in the molecular cloud, assuming N3 is located in the GC. In this case the compact source would be enveloped in

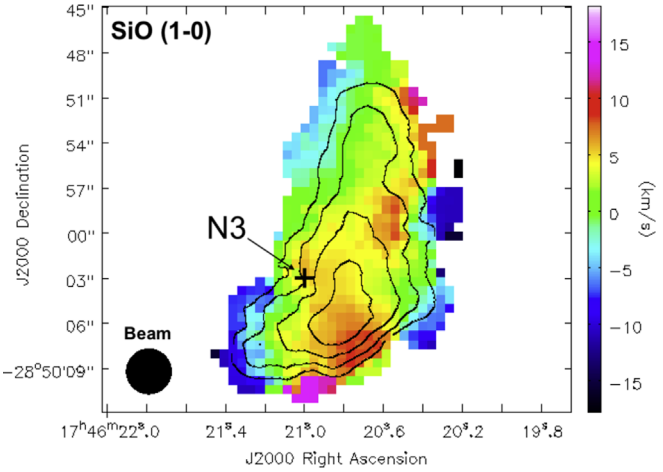

Figure 5. Intensity-weighted velocity distribution (moment 1) of the N3 molecular cloud in SiO (1−0) emission from Ludovici et al. (2016). Contours show the integrated intensity (moment 0) of the SiO (1−0) at 20%, 40%, 60%, and 80% of the peak intensity (1.184 Jy beam^{-1} km s^{-1}).

molecular material and surrounded by the two-velocity components, discussed in Section 3.3.1, which could represent the near and far sides of the cloud. If N3 was a massive compact object the broad line width on the 0.01 pc size scale could be caused by the gravitational interaction between the gas and N3. Additionally, the morphology of the cloud, which appears to wrap around N3 (e.g., see Figure 5), may support this claim.

However, this described scenario disagrees with our H_2CO observations presented in Section 2. The two H_2CO absorption components are comparable to the two-velocity components averaged over the entire cloud (see the discussion in Section 3.3.1, Figure 4, and Table 2). The detection of absorption in both velocity components is consistent with the cloud being located in front of the N3 point source. The lack of a distinct secondary component in the CH_3OH transition could be due to differences in the gas properties between the two-velocity components (e.g., temperature). The residuals of the CH_3OH fitted spectrum are consistently negative between −10 and 0 km s^{-1}, hinting there could be a secondary component at this velocity range. However, the depth of this feature is at the 1σ level (∼2 K). Higher-sensitivity 6.7 GHz CH_3OH observations are needed to determine if this feature is a secondary absorption component. Additional follow-up observations at high spectral resolution in multiple transitions are also necessary to investigate possible causes for the variation in the gas properties in the two components of the cloud.

4. Summary

We present the detection of 6.7 GHz CH_3OH and 4.8 GHz H_2CO absorption toward the "N3" point source (see Section 3.1). The N3 point source is located toward the Galactic Center Radio Arc and is unresolved at an angular size of 0.″26 (<0.01 pc for a source in the GC, Ludovici et al. 2016). The detection of the absorption features indicates that some of the gas in the N3 molecular cloud is located *in front* of the point source N3 (Section 3.2). We also compare the kinematics of this absorption feature to the Larson line width–size relationship (Section 3.3). The Larson line width–size relationship suggests a velocity dispersion of 0.26 km s^{-1} for a

size scale of 0.01 pc. However, fitting the kinematics of the CH_3OH absorption feature indicates a velocity dispersion of 3.8 km s^{-1}, an order of magnitude higher then predicted. We argue this relatively broad velocity dispersion is caused by turbulence along the depth of the cloud, where the thickness of the cloud is larger then the cross section of the absorption feature. The analysis presented in Section 3.3.1 suggests the N3 cloud has a thickness of roughly 1 pc. Furthermore, the detection of 4.8 GHz H_2CO absorption toward both velocity components of the N3 cloud is consistent with N3 being located behind the entire cloud. Therefore, N3 could be a background AGN.

A.T.B. would like to acknowledge the funding provided from the European Union's Horizon 2020 research and innovation programme (grant agreement No. 726384). D.L. would like to thank Katana Colledge for her assistance in setting up the VLA observations used to make the H_2CO data cube. We would also like to thank Dr. Alexei Kritsuk and Dr. Juergen Ott for their helpful insight on these results. N.B. would also like to thank Dr. Drew Medlin at NRAO for assisting with pipeline calibration. We would also like to thank the anonymous reviewer for their helpful comments on this work.

Software: CASA (International Consortium Of Scientists 2011); *pyspeckit* (Ginsburg & Mirocha 2011).

ORCID iDs

Natalie O. Butterfield https://orcid.org/0000-0002-4013-6469
Adam Ginsburg https://orcid.org/0000-0001-6431-9633
Dominic A. Ludovici https://orcid.org/0000-0002-8631-6457
Ashley Barnes https://orcid.org/0000-0003-0410-4504
Riley Dunnagan https://orcid.org/0000-0002-9431-5067
Mark R. Morris https://orcid.org/0000-0002-6753-2066

References

Abuter, R., Amorim, A., Anugu, N., et al. 2019, A&A, 625, 10
Butterfield, N., Lang, C. C., Morris, M., Mills, E. A. C., & Ott, J. 2018, ApJ, 852, 11
Caswell, J. L., Fuller, G. A., Green, J. A., et al. 2010, MNRAS, 404, 1029
Ginsburg, A., Henkel, C., Ao, Y., et al. 2016, A&A, 586, A50
Ginsburg, A., & Mirocha, J. 2011, PySpecKit: Python Spectroscopic Toolkit, v. 0.1.20, Astrophysics Source Code Library, ascl:1109.001
Heyer, M., Krawczyk, C., Duval, J., & Jackson, J. M. 2009, ApJ, 699, 1092
Impellizzeri, C. M. V., Henkel, C., Roy, A. L., & Menten, K. M. 2008, A&A, 484, L43
Indebetouw, R., Brogan, C., Chen, C.-H. R., et al. 2013, ApJ, 774, 73
International Consortium Of Scientists 2011, CASA: Common Astronomy Software Applications, v.5.0 Astrophysics Source Code Library, ascl:1107.013
Kauffmann, J., Pillai, T., Zhang, Q., et al. 2017, A&A, 603, A89
Larson, R. B. 1981, MNRAS, 194, 809
Lu, X., Mills, E. A. C., Ginsburg, A., et al. 2019, ApJS, 244, 35
Ludovici, D. A., Lang, C. C., Morris, M. R., et al. 2016, ApJ, 826, 218
Menten, K. M. 1991, ApJL, 380, L75
Mills, E. A. C. 2017, arXiv:1705.05332
Mills, E. A. C., & Morris, M. R. 2013, ApJ, 772, 105
Oka, T., Hasegawa, T., Sato, F., et al. 2001, ApJ, 562, 348
Pandian, J. D., Leurini, S., Menten, K. M., Belloche, A., & Goldsmith, P. F. 2008, A&A, 489, 1175
Rickert, M., Yusef-Zadeh, F., & Ott, J. 2019, MNRAS, 482, 5349
Shetty, R., Beaumont, C. N., Burton, M. G., Kelly, B. C., & Klessen, R. S. 2012, MNRAS, 425, 720
Staguhn, J., Arendt, R. G., Dwek, E., et al. 2019, ApJ, 885, 72
Whiteoak, J. B., & Gardner, F. F. 1979, MNRAS, 188, 445
Yusef-Zadeh, F., & Morris, M. 1987, AJ, 94, 1178